Journal of Volcanology and Geothermal Research 391 (2020) 106365

Contents lists available at ScienceDirect

Journal of Volcanology and Geothermal Research

journal homepage: www.elsevier.com/locate/jvolgeores

Magma "bright spots" mapped beneath Krafla, Iceland, using RVSP imaging of reflected waves from microearthquakes

Doyeon Kim [a,*], Larry D. Brown [a], Knútur Árnason [b], Ólafur Gudmundsson [c], Kristján Ágústsson [b], Ólafur G. Flóvenz [b]

[a] Earth and Atmospheric Sciences, Cornell University, Ithaca, NY, United States
[b] Iceland Geosurvey (ISOR), Reykjavik, Iceland
[c] Department of Earth Sciences, Uppsala University, Uppsala, Sweden

ARTICLE INFO

Article history:
Received 16 December 2017
Received in revised form 6 February 2018
Accepted 25 April 2018
Available online 28 April 2018

Keywords:
Magma
Microearthquake
Reflection imaging
Vertical Seismic Profiling
Magma chamber model

ABSTRACT

The geometry and distribution of magma in the crust remain controversial topics with recent studies questioning the role of large magma chambers. In this investigation, high-resolution 3D reflection images of crustal discontinuities beneath the Krafla geothermal field in northern Iceland were generated by applying Vertical Seismic Profiling (VSP) techniques adapted from reflection seismology to microearthquake data. Exceptionally large amplitude reflections (bright spots) at a depth of 2.1 km correlate with rhyolitic magma encountered in the IDDP-1 borehole. Although similarly bright reflectors at about 4 km correspond in depth to the top of an inferred magma chamber from previous seismic studies, the scattered reflectivity that persists beneath this deeper reflector argues for a distributed magma system rather than a large feeder chamber.

1. Introduction

The Krafla volcano hosts a large geothermal system that is one of the most studied energy fields in Iceland, with geothermal exploration dating back to the early 1970's (Sveinbjornsdottir et al., 1986). Krafla sits in the Northern Volcanic Zone of Iceland and the historical record includes episodic rifting events in the region every 100–150 years (Björnsson and Saemundsson, 1977). The most recent such rifting event documented in the region is during the Krafla-Fires 1975–1984 (Einarsson, 1991). Krafla's magmatic plumbing regained its attention in 2009 when two geothermal boreholes, KG-39 and IDDP-1 unexpectedly encountered magma at depths of 2062 m and 2104 m, respectively, a rare event in drilling history (Mortensen et al., 2010; Elders et al., 2014b). These boreholes have received substantial attention as a model for superheated geothermal power generations (Elders et al., 2014a).

A number of geophysical techniques, especially magnetotelluric (MT) and seismic, have been widely used to detect and delineate magma at depth. Examples of recent MT efforts in Iceland have shown the inferred magma body beneath Hengill and Krafla geothermal area (Árnason et al., 2009, 2010). Other studies elsewhere to image magma include the detection of extensive fluid distribution beneath the Tibetan Plateau (Wei et al., 2001; Unsworth et al., 2005), and the combination of partial melt and fluids of Altiplano-Puna magma body (Comeau et al., 2015). Both natural and artificial seismic sources have been used to image magma. Tomographic imaging using both local earthquakes and teleseismic sources are probably the best known (e.g., Lees, 2007). Ambient noise techniques have also been applied to map magma at depth, including attempts to detect temporal variations in the seismic velocity within magma systems (e.g., Brenguier et al., 2007; Jaxybulatov et al., 2014). Another widely used passive seismic technique, receiver function mapping of intracrustal convertors, has also been used to detect and map crustal magma (e.g., Sheetz and Schlue, 1992; Zandt et al., 2003; Wilson et al., 2005). However the highest resolution images interpreted to be of magma come from controlled source reflection surveys (e.g., Brown et al., 1979; de Voogd et al., 1986; Brown et al., 1996; Kent et al., 2000). A drawback of controlled source reflection imaging is the relatively high cost of artificial sources. Conversely, conventional passive methods that rely upon teleseismic sources lack resolution at intracrustal scales (Cassidy, 1992). Here, we apply a technique normally used with controlled sources to obtain high resolution seismic imaging using natural sources, in this case crustal microearthquakes.

Of particular relevance to this study are previous efforts to detect magma using reflected waves from earthquake sources. Sanford and Long (1965) reported an anomalously strong, late arriving S wave from the midcrust on microearthquake records near Socorro, New Mexico. These phases were subsequently interpreted as the reflected SxS and PxS waves from an extensive magma layer beneath the Rio

* Corresponding author at: 112 Hollister Drive, Cornell University, Ithaca, NY 14853-1504, United States.
E-mail address: dk696@cornell.edu (D. Kim).

https://doi.org/10.1016/j.jvolgeores.2018.04.022
0377-0273/

Grande Rift, now commonly referred to as the Socorro Magma Body (SMB; e.g., Sanford et al., 1973; Balch et al., 1997). This work inspired the interpretation of similar anomalous S waves on microearthquake records in Japan as reflections from magma beneath several volcanic systems. (Hasegawa and Yamamoto, 1994; Matsumoto and Hasegawa, 1996). Byerly et al. (2010) also used microearthquakes to search for magma beneath Montserrat in the Caribbean.

Inamori et al. (1992) were the first to correct the reflection times of anomalous midcrustal reflected S waves for the depth of the source, in this case for the western Nagano Prefecture in Japan. Here, the proper travel time and lateral position corrections are equivalent to those inherent in Vertical Seismic Profiling (VSP), a technique widely used in the oil exploration industry for imaging sedimentary strata using sources or receivers in boreholes. Quiros et al. (2017) first applied VSP processing to aftershock recordings of the August 23 2011, 5.8 Mineral Virginia earthquake to produce high resolution 3D images of crustal structure in the hypocentral region of that event. In this study, we apply similar VSP approach to reflected phases on recordings of microearthquakes generated by geothermal activities near Krafla, Iceland, to image the underlying volcanic-geothermal system.

2. Data and methods

Although Krafla has been the subject of a number of geophysical studies (e.g., Brandsdóttir and Menke, 1992; Arnott and Foulger, 1994; Darbyshire et al., 2000; Árnason et al., 2009), none detected the magma that was encountered during drilling. However, recently Kim et al. (2017) used microearthquake seismograms collected by a dense temporary array, deployed within a project named Deep Roots of Geothermal systems (DRG) (Fig. 1), to image the upper crust using seismic interferometry. This technique was based on redatuming surface ghost reflections from upgiong waves from microearthquakes to simulate surface source Common MidPoint (CMP) reflection profiles. Virtual reflection profiles produced seismic sections with reflections, some of which correspond to the position of the magma encountered in IDDP-1. Here we use the same dataset to produce 3D reflection images of the subsurface by applying the VSP methodology to seismic waves initially propagating downward from the microearthquake sources.

The DRG network consists of 20 three-component seismometers with Lennartz 0.2 Hz sensors installed on two profiles, one passing close to IDDP-1 (Fig. 1a). Station spacing was 200 m and the data were sampled at 200 Hz (Fig. 1a). The data were acquired over a two-month period (July to August) in 2014. Relatively continuous seismic activity was observed with average focal depths of about 2 km. A total of 989 microearthquakes (magnitude $M_L < 2$) were located using both temporary and permanent seismic stations (ISOR, 2014). A simple least-square-inversion based algorithm (Bratt and Bache, 1988) was applied with an *a prioiri* velocity model from a refraction profile within and close to the caldera (blue, Fig. 4d). We visually examined and selected the records of 120 events that showed clear coherent phases between the direct P and S wave arrivals (e.g., Fig. 1b). The horizontal and vertical uncertainties of locations of these events are on the order of 500 m and 1 km, respectively (personal communication, ISOR).

In order to minimize possible complications (e.g., polarity changes) due to variations in focal mechanisms of the microearthquakes, we only included records in which the polarity of the prominent reflected phases was consistent among events. The selected recordings were then band-pass filtered between 2 Hz and 16 Hz to emphasize body waves and normalized by the root-mean-square amplitude for each microearthquake. Incorporation of higher frequencies resulted in traces too noisy to be useful in our analysis. The example shown in Fig. 1b exhibits a strong coherent phase that arrives shortly after the direct P wave. As implied by its PzP label, we interpret this arrival as a reflection of downgoing energy from an interface beneath the hypocenter (Fig. 2b). Here, we used vertical component records to minimize contributions from S wave energy, and leave similar treatment of S waves for future analysis.

The VSP technique has a long history in the oil exploration industry (Hardage, 2000). It is widely used to tie surface reflection profiles to lithology (Balch and Lee, 1984). It is usually done with sources at the surface and receivers in a borehole (Fig. 2a). Alternatively, receivers can be placed at the surface and the sources placed in the borehole (reverse VSP or RVSP). If surface sources or receiver arrays extend away from the borehole, 2D and 3D reflection images can be made of the volume between them (Dillon and Thomson, 1984).

When multiple sources and/or multiple receivers are available, signal stacking can be applied. This is the basis of the well-known CMP reflection technique (Fig. 2c) routinely applied to multichannel recordings of surface sources (Yilmaz, 2001). However, the raypaths associated with subsurface sources are more complex. The CMP assumption for reflection points is no longer valid and a more complicated Common Reflection Point (CRP) treatment is needed for effective signal

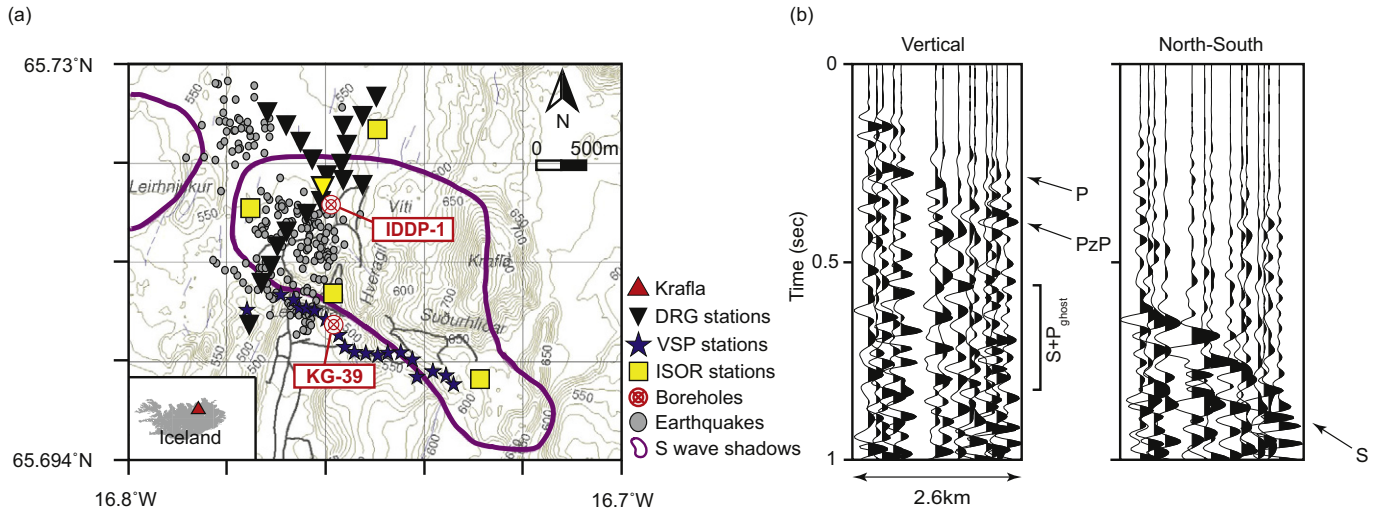

Fig. 1. (a) Study area in the Krafla geothermal field showing the locations of the IDDP-1 and KG-39 boreholes (red circles) within the DRG seismic network (black triangles). Note VSP stations used in the IMAGE field campaign (blue stars) and permanent ISOR stations (yellow squares). Microearthquakes discussed in the main text are illustrated with gray circles. Purple lines indicate boundaries of regions where high S wave attenuation was mapped during 1975–1984 Krafla rifting events (Eniarsson, 1978). The DRG station highlighted in yellow was used for the waveform analysis in Fig. 5. (b) A sample microearthquake recording from DRG network. A reflected phase (PzP) is evident between P and S wave.

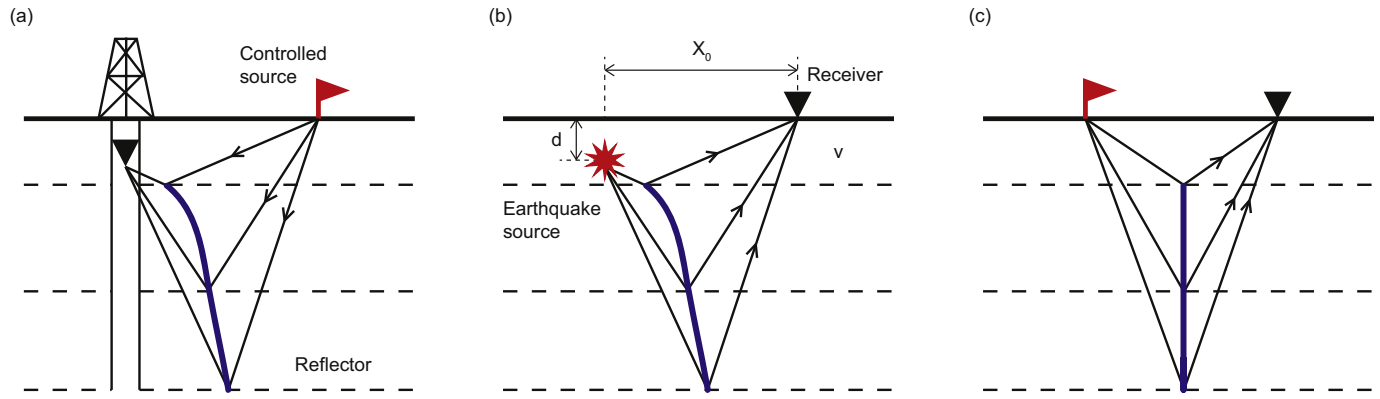

Fig. 2. (a) Representative raypath geometry for conventional VSP survey, (b) RVSP using earthquake as a source, and (c) conventional surface source (CMP) seismic reflection survey.

stacking. Reflected energy from the subsurface source must be mapped into its correct reflection point in both space and time (i.e., depth). For a constant velocity medium with horizontal interfaces (e.g., Fig. 2b), the following Eqs. (1) and (2) define the mapped CRP location of x_i and z_i, respectively with a given time sample, t_i:

$$x_i = \frac{X_0}{2}\left(1 - \frac{d}{\sqrt{(t_i v)^2 - {X_0}^2}}\right) \quad (1)$$

$$z_i = \frac{1}{2}\left(\sqrt{(t_i v)^2 - {X_0}^2} + d\right) \quad (2)$$

where X_0 is the lateral offset, v, the velocity of a layer, and d, depth of the source (Dillon and Thomson, 1984). The reflected energy in the RVSP geometry will map onto a curved path in 3D space. The blue curves in Fig. 2 illustrate the mapping of reflection points from a source at depth (Fig. 2a and b) as compared with the conventional CMP mapping for surface sources (Fig. 2c). Energy from different sources (earthquakes) illuminating a given CRP can then be summed. Note that the CRP path for the RVSP geometry approaches that of the CMP as the depth of the reflecting interface increases.

We initially computed RVSP images using individual microearthquakes that show clear reflection phases. The reflection phases (e.g., PzP) of these microearthquakes were mapped into three dimensional CRP bins using a simplified 1D velocity model (Fig. 4d) derived from a previous active source VSP survey (IMAGE, 2016) and stacked. The data were insufficient to robustly define a more complex 3D velocity model.

3. Results and discussion

Fig. 3 shows examples of individual (single fold) images after application of RVSP moveout. These images represent the moveout-corrected traces of the subsection of the in-line and the cross-line profiles that are highlighted on the map view. The most prominent feature of these sections is a persistent, strong, subhorizontal reflector at a depth of about 2.4 km in the vicinity of the IDDP-1, slightly deeper than the depth of the magma encountered in the borehole (2.1 km). The apparent difference in depth (Fig. 4a) is on the order of those expected from uncertainties from earthquake locations and/or the velocity model used to convert time-to-depth. For example, a simple shift made to the location of earthquake #1 in Fig. 3a would easily make a very close correspondence between the depth of the reflector and the depth at which magma was encountered in the IDDP-1 borehole (Fig. 4b). Likewise, uncertainties in the appropriate velocity structure in the area will result in corresponding uncertainties in the depth of any reflector (Fig. 4c). Given these uncertainties, it is reasonable to infer that the bright reflection appearing at 2.4 km on the RVSP image is from the same magmatic body encountered by IDDP-1 borehole. The data show that the reflector continues at least 1 km westward from the well at roughly the same depth (Fig. 3a). The magma interpretation is supported by the anomalous amplitude of this reflector (rightmost panel in Fig. 3). Local occurrences of unusually large reflection amplitudes are often referred to as "bright spots". Such bright spots were first associated with gas pockets in hydrocarbon reservoirs (e.g., Sheriff, 1975) but the terminology has also been applied to anomalous reflections interpreted to be from magma bodies or magma related fluids (Brown et al., 1979; de Voogd et al., 1986; Brown et al., 1996; Kent et al., 2000). The high amplitudes in this case cannot be attributed to critical reflection as the angles of incidence involved are <20°. Reflection polarity can sometimes be useful for discriminating a solid-liquid interface (e.g., magma or brines) from a solid-solid interface with an unusually large seismic impedance contrast (Brown et al., 1996). A polarity reversal (e.g., from positive to negative) is expected for a simple transition from solid to liquid. However, using polarity as a discriminant is in general difficult due to complicating factors such as interference of reflections from multiple interfaces, geometrical focusing, lateral velocity heterogeneity and source radiation patterns (e.g., focal mechanisms). In this case, we found the polarity variations to be inconclusive.

Another prominent reflector is seen on the profiles in Fig. 3b at a depth of 3.9 km, well beneath the bottom of the boreholes. Again, the strong amplitude of this deep event is consistent with, if not confirmation of, a fluid reflector (e.g., magma, entrapped brines, steam, CO_2, or SO_2). This reflector lies near the edge of the attenuating body mapped during 1975–1984 Krafla rifting events (Einarsson, 1978) as shown by purple lines in Fig. 3. Other observations have been interpreted to suggest the existence of a simple magma chamber with its top near 3 km depth (e.g., Brandsdóttir and Menke, 1992; Arnott and Foulger, 1994; Brandsdóttir et al., 1997). A recent MT and microseismic study also indicates the presence of magma chamber at similar depth (Friðleifsson et al., 2014). Furthermore, P wave reflections observed from the recent IMAGE VSP field campaign suggest the presence of magma at a depth of about 3.5 km. These observations thus support an interpretation of our 4 km reflector as the top of a magma accumulation. However, little apparent energy is shown at this depth on the profiles in Fig. 3a. This suggests that whatever the reflector, it has piecemeal lateral continuity, inconsistent with a single, laterally extensive magma chamber.

CRP binning (50 × 50 m) of data from 120 selected microearthquakes was used to produce a stacked, 3D seismic volume (Fig. 6). The bright reflector at 2.4 km is still prominent on the cross-line section, but less continuous on the in-line section than on the single fold sections. Optimal 3D reflection imaging requires recording of multiple sources with a dense 2D surface array to achieve adequate redundancy and uniform subsurface sampling (e.g., Brown, 2011). However, we only have a pair of 2D recording profiles available. Since relatively few seismic stations were deployed along the in-line direction, the resulting

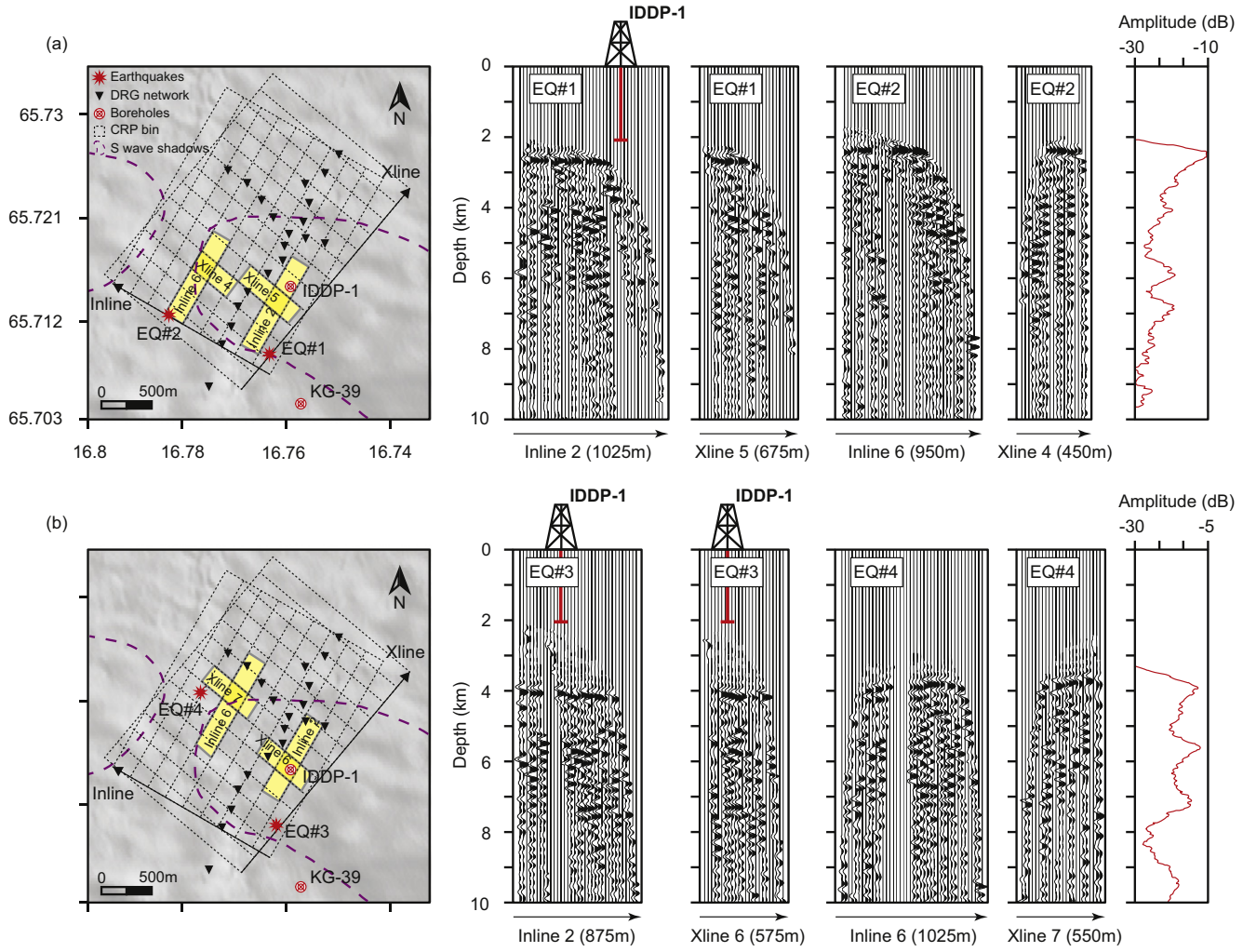

Fig. 3. RVSP images using individual microearthquakes. Seismic traces correspond to the highlighted CRP bins on the map. To maximize stacking fold within the bins, two separate grids are made that are parallel to the seismic arrays. Red vertical lines displayed on RVSP images represent the depth of the drilled magma by IDDP-1 borehole. Two distinct reflectors are evident: (a) a reflector at 2.4 km depth where magma was encountered by IDDP-1 and (b) a deeper reflector at a depth of about 3.9 km. The seismic sections are displayed with horizontal exaggeration of 4 to 1. Amplitude decay curves at right were computed as $20\log_{10}$amplitude of the average trace.

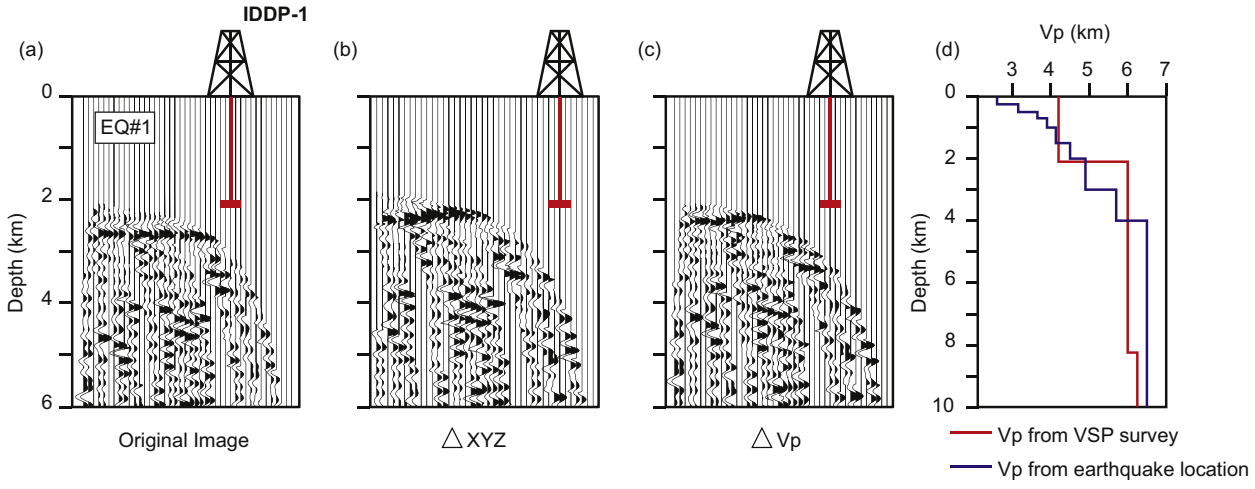

Fig. 4. Correlation of seismic image with IDDP-1 borehole position of known magma. Red vertical lines displayed in (a)–(c) represent the depth of the drilled magma by IDDP-1 borehole. (a) RVSP image using reported hypocenter of earthquake #1 as shown in Fig. 3a. (b) RVSP image after shifting the location of earthquake #1 by 250 m, 180 m, and 330 m in latitude, longitude and depth, corresponding to the reported position uncertainties for this event, respectively. (c) RVSP image produced by the velocity model indicated in blue instead of that derived from the VSP survey (d). (d) Velocity variations derived from the local VSP survey (red) compared with those used for inverting the microearthquake locations (blue).

images of the cross-line sections are generally higher quality than in-line sections. Reflections from 4 to 8 km depth are generally discontinuous and reverberatory. The reverberatory character could be due, at least in part, to errors in the earthquake source locations blurring the stacked image (e.g., Fig. 4a and b), or perhaps to S wave contamination (e.g., S-to-P converted phases). However, the 3D control provided by the crossing 2D lines argues against "sidewipe" (out of plane arrivals) as a major contributing factor. Note that the free-surface multiple (ghost) from the reflector at 2.1 km depth, which was used by Kim et al. (2017) for imaging via interferometry, would be expected to arrive at about 6 km depth. However, no prominent event is evident at this depth, consistent with our expectation that while multiple energy might be present on the single fold sections, it should be degraded by the stacking process. We interpret the laterally discontinuous nature of the deeper reflections to be direct evidence of the discontinuous nature of the reflecting bodies themselves.

We interpret that the strongest reflections correspond to the large change in acoustic impedance that would be expected at a solid-to-fluid interface. The identity of the fluid is open to speculation. Magma is the most obvious candidate, but other magma related fluids (e.g. brines, steam, CO_2, or SO_2) could also be a factor (Makovsky et al., 1999). There is no clear evidence of a distinct "bottom" bright spot corresponding to any of these events. These could simply mean that the base of each fluid accumulation is too gradual to give rise to a reflection at these wavelengths. Alternatively, the fluid bodies may be thin, with the observed reflections being composites from the top and bottom of the unit. This latter interpretation is supported by the modeling of the seismic waveform shown in Fig. 5, where an averaged trace of an earthquake cluster recorded by a single DRG station is compared with synthetic records generated by the SPECFEM2D code (Tromp et al., 2008). We modeled the reflection waveforms at the drilled magma depth with thickness varying from 25 to 1000 m (highlighted zone, Fig. 5b). A distinct top and bottom (circled in blue) reflection is evident in the synthetics for the thicker magma layer models (e.g. 100, 500 and 1000 m). For smaller thicknesses, a composite waveform marks the magma layer. Comparison of the observed seismic trace in Fig. 5a with the synthetics in 5b suggests a) that p wave reflections from the bottom of a thick magma layer could be obscured by S waves, and b) that observed reflection which we interpret to be from the magma layer is a poor match to the synthetics for a composite layer if P waves alone are used. A better match is seen between the observed average trace in Fig. 5a with the synthetic in Fig. 5c, which includes converted phases from the two layers.

The stacked seismic sections (e.g. Fig. 6) indicate that the crust is characterized by a suite of strong, short reflectors, with no clear correlation to the overlying shallow bright spot that we associated with the drilled magma. A thick magma layer, whether shallow or deep, would be expected to strongly attenuate any through-going seismic waves, making observation of reflections, P or S, from either its base or underlying magma bodies problematic. We therefore speculate that the prominent, albeit discontinuous, reflectivity between 3 and 6 km on the stacked sections (Fig. 6a) is evidence of a distributed magma system, rather than a simple large, upper crustal magma chamber at these depths beneath Krafla. The rift context, not to mention linear eruptive geometries like the Krafla-Fires, would suggest dikes as a major mode of emplacement. However, if these reflections were from the top of dikes, we might expect some indication of enhanced attenuation below and perhaps diffractions from the top "edges". These observed reflection segments instead suggest a series of sill-like, intermittent magma lenses at various depths (Fig. 6d). 3D reflection depth slices could perhaps distinguish sill vs. dike geometries that may not be apparent in our 2D images. However, the uneven spatial coverage associated with the irregular source distribution coupled with the linear DRG profiles does not provide sufficient crossline coverage to clarify this issue. Of course a suite of sills on the reflection image implies a corresponding, and perhaps less seismically visible, set of feeder dikes (e.g. Fig. 6d).

Distributed magma rather than large magma chambers has also been argued from seismic tomography (Jeddi et al., 2016), and

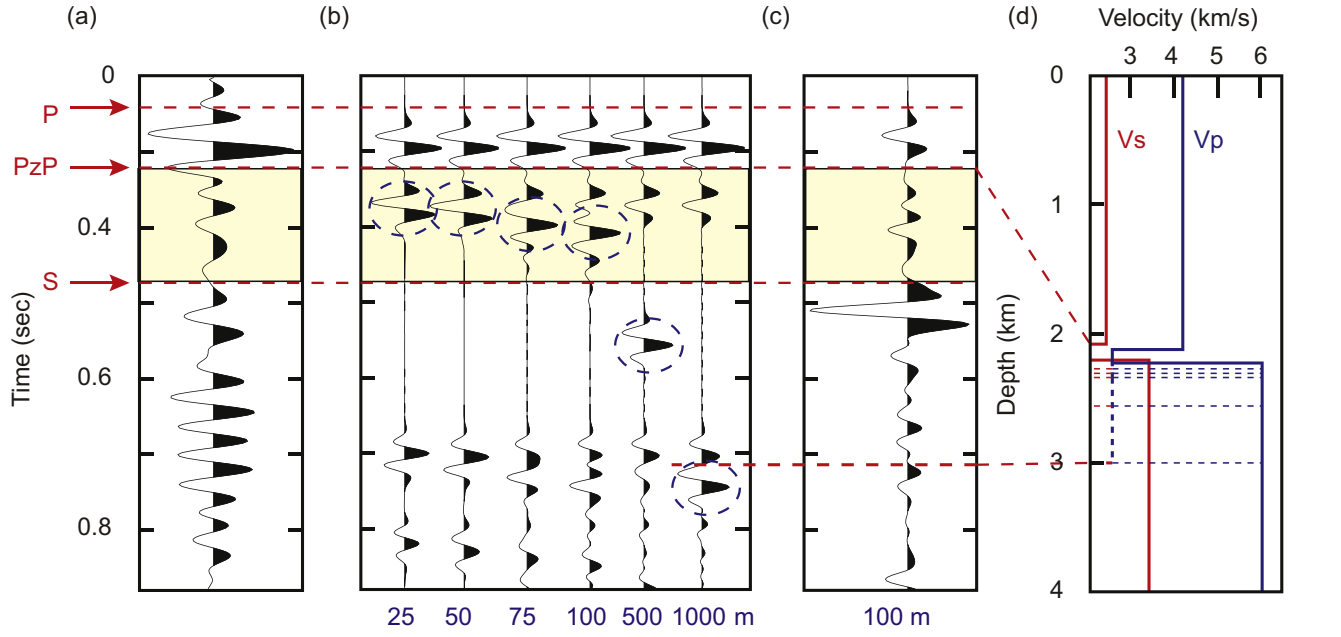

Fig. 5. Comparison of the observed bright spot reflection from shallow (ca 2 km) feature in data with synthetic responses from a simple magma layer. (a) The average amplitude of recordings from five adjacent earthquakes as recorded by a single DRG station (yellow triangle, Fig. 1a). This average trace has been filtered by the same 2–16 Hz filter used in our previous described analyses. Note that the amplitude of the S wave is subdued by destructive interference from stacking. (b) Synthetic seismograms produced by a 10 Hz Ricker wavelet propagating through the acoustic model shown as blue line in (d). Blue circles indicate P wave reflections from the base of magma layer on the synthetic traces. (c) Same as a 100 m thick magma layer in (b) with full waveforms containing both P and S waves. The highlighted zone is bounded by the theoretical arrival times of PzP and S wave in the model. (d) Velocity models used in (b) and (c). Dotted lines correspond to different thickness of the low velocity layered used in (b) and (c), as shown at the bottom of each trace. The assumed P wave velocity for the magma body is based on the lab measurements of Murase and Mcbirney, 1973.

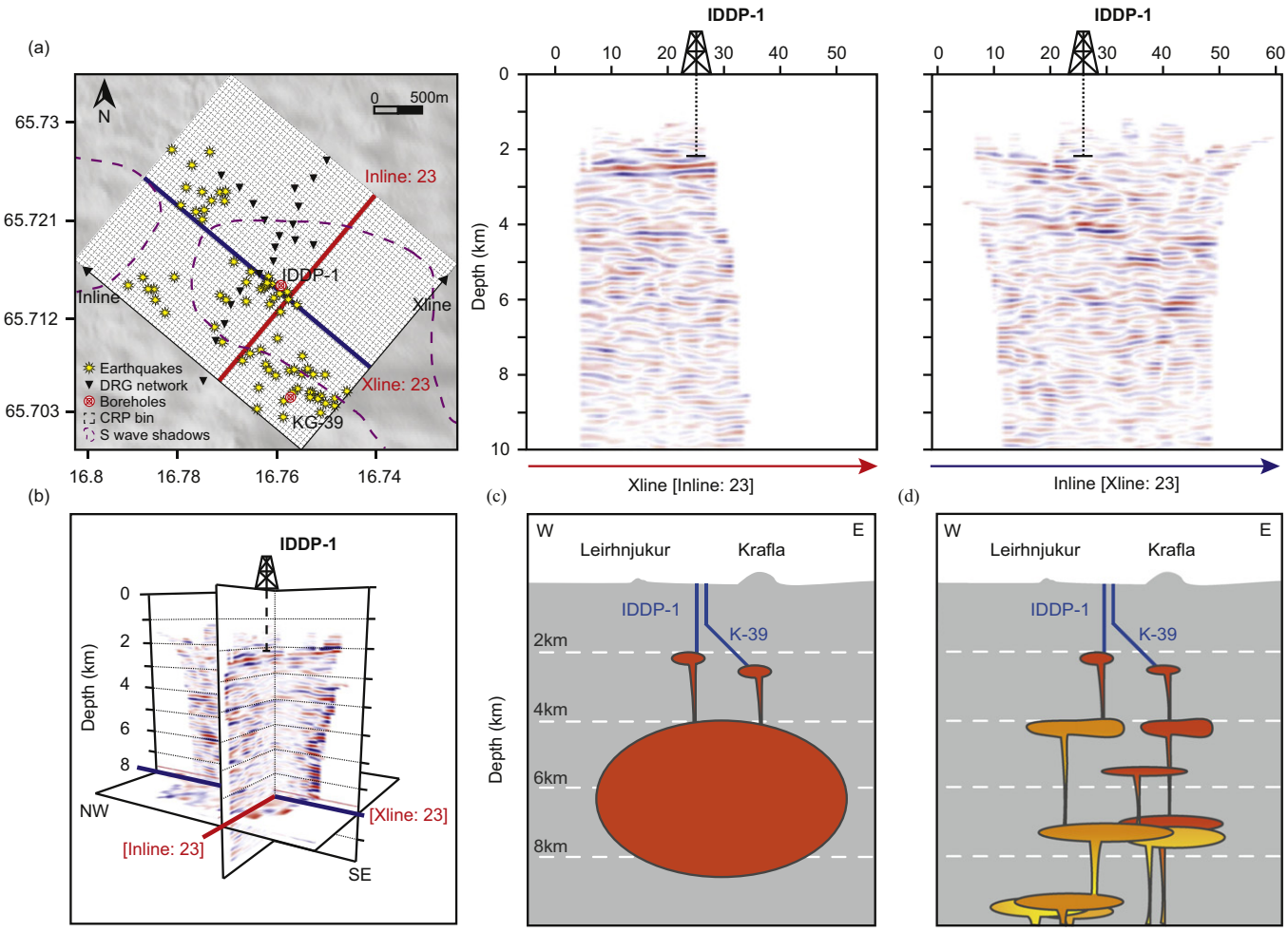

Fig. 6. (a) 3D RVSP stack using 120 earthquakes. Red and blue lines on map to the left indicate the layout of the vertical seismic sections to the right. Earthquake locations are indicated with yellow stars. The seismic sections are displayed with horizontal exaggeration of 3 to 1. (b) 3D fence display of the images in (a). (c) and (d) Two contrasting concepts of magma beneath Krafla: a large volume of pervasively molten magma vs. a distributed suite of smaller magma accumulations. The different colors are intended to suggest different generations of intrusion.

microseismicity (Tarasewicz et al., 2012; Greenfield and White, 2015). Cooper et al. (2016) interpreted petrological data from the 1975–1984 Krafla rifting events as not being products of crystallization from a large, single host liquid, but from diverse magma sources within the crust. As discussed by Cashman et al. (2017), the details of a distributed magma system may simply be too small to be resolved by many of the geophysical methods previously used to image the velocity and conductivity anomalies expected from such a distribution. Marjanović et al. (2014) have likewise argued that the concept of a "mush" volume at fast and intermediate spreading-rate ridges (Detrick et al., 1987; Kent et al., 1993) has been challenged both by newer, high resolution seismic reflection data as well as analogy to mapping of exposed sections of former oceanic crust, both of which indicates the "mush zone" is a complex suite of sill-like magma lenses.

As described earlier, the seismometer array used in this experiment is not a true 3D recording deployment, which would involve an areal grid of instruments at comparably dense spacing in both dimensions (e.g., Walton, 1972). Our images do not uniformly sample the subsurface in 3D space. Such a restricted surface coverage undoubtedly limits the quality of the resulting image and introduces ambiguity in interpretation of structural details. An adequate areal array would require the deployment of hundreds of seismometers. Such a "large N" array for passive recording has recently become more feasible by the development of nodal recordings systems by the oil exploration industry (e.g. Lin et al., 2013).

Other factors may further limit the image quality. For example, the RVSP technique requires accurate knowledge of earthquake location and origin time. Source location errors may blur reflections on stacked images (Fig. 6). We note that "large N" arrays would also provide more precise determination of both subsurface velocity variations (Davenport et al., 2015) and hypocentral locations (e.g. Quiros et al., 2015).Variations in amplitude of the downgoing waves due to variations in the source magnitude and focal mechanism can cause destructive or constructive interference when stacked. Contributions from S or converted phases, if present, could obscure or masquerade as P wave reflection energy. However, the near vertical geometry of reflection raypaths from the earthquakes to the DRG stations argues against significant SzS or mode converted reflections. Complications due to variations in the source function (rupture history) are likely to be minimal since the magnitude of the microearthquakes is quite small.

4. Conclusions

We adapt conventional VSP techniques to image reflectors beneath the Krafla geothermal field using microearthquakes associated with geothermal activity in the upper crust. An unusually strong reflector is mapped at the depth corresponding to the magma encountered by the by IDDP-1 drillhole. Similar strong coherent reflectors at depths ranging from 4 to 6 km are likewise interpreted as magma bodies. Although 4 km corresponds to the top of a magma reservoir previously inferred from lower resolution geophysics, the reflection image indicates a

distributed system of smaller magma sills rather than a large pervasively molten feeder chamber. Exploiting earthquakes as sources in RVSP imaging is attractive because it can yield resolution comparable to controlled source CMP reflection imaging without the cost or limitations of artificial sources. Lower cost may also translate into feasibility of time lapse reflection imaging with special relevance to monitoring active subsurface processes such as magma movement and volcanism. The availability of new "large N" passive seismic array technology makes this technique a powerful new tool for imaging geothermal systems.

Acknowledgments

We would like to acknowledge our appreciation to ISOR, GEORG, and the National Power Company in Iceland for providing data and Schlumberger for providing 3D VSP-CDP mapping module in Vista 3D software package. We thank Muawia Brazangi and Diego Quiros for constructive comments on the manuscript. We are also appreciative of many helpful suggestions from Dr. Michal Malinowski in his review of the earlier draft of this work. Doyeon Kim was supported by NSF grant (Grant No. 966045) as a part of Integrative Graduate Education and Research Traineeship (IGERT) program at Cornell University. The DRG seismic data is open and available upon request to ISOR (isor@isor.is or http://www.geothemal.is).

References

Árnason, K., Vilhjálmsson, A.M., Björnsdóttir, Þ., 2009. A Study of the Krafla Volcano Using Gravity, Micro Earthquake and MT Data. Iceland GeoSurvey Report ÍSOR-2009/067 (Reykjavik, Iceland, 66 pp).

Árnason, K., Eysteinsson, H., Hersir, G.P., 2010. Joint 1D inversion of TEM and MT data and 3D inversion of MT data in the Hengill area, SW Iceland. Geothermics 39 (1), 13–34.

Arnott, S.K., Foulger, G.R., 1994. The Krafla spreading segment, Iceland: 1. Three-dimensional crustal structure and the spatial and temporal distribution of local earthquakes. J. Geophys. Res. Solid Earth 99 (B12), 23801–23825.

Balch, A.H., Lee, M.W., 1984. Vertical Seismic Profiling: Technique, Applications, and Case Histories. IHRDC Press, Boston, MA.

Balch, R.S., Hartse, H.E., Sanford, A.R., Lin, K., 1997. A new map of the geographic extent of the Socorro mid-crustal magma body. Bull. Seismol. Soc. Am. 87 (1), 174–182.

Björnsson, A., Saemundsson, K., 1977. Current rifting episode in north Iceland. Nature 266, 318–323.

Brandsdóttir, B., Menke, W.H., 1992. Thin low-velocity zone within the krafla caldera, ne-Iceland attributed to a small magma chamber. Geophys. Res. Lett. 19 (24), 2381–2384.

Brandsdóttir, B., Menke, W., Einarsson, P., White, R.S., Staples, R.K., 1997. Færoe-Iceland Ridge Experiment 2. Crustal structure of the Krafla central volcano. J. Geophys. Res. Solid Earth 102 (B4), 7867–7886.

Bratt, S.R., Bache, T.C., 1988. Locating events with a sparse network of regional arrays. Bull. Seismol. Soc. Am. 78 (2), 780–798.

Brenguier, F., Shapiro, N.M., Campillo, M., Nercessian, A., Ferrazzini, V., 2007. 3-D surface wave tomography of the Piton de la Fournaise volcano using seismic noise correlations. Geophys. Res. Lett. 34 (2).

Brown, A.R., 2011. Interpretation of three-dimensional seismic data. Society of Exploration Geophysicists and American Association of Petroleum Geologists Retrieved from. https://doi.org/10.1190/1.9781560802884.index.

Brown, L.D., Krumhansl, P.A., Chapin, C.E., Sanford, A.R., Cook, F.A., Kaufman, S., Oliver, J.E., Schilt, F.S., 1979. COCORP Seismic Reflection Studies of the Rio Grande rift, Rio Grande Rift: Tectonics and Magmatism. pp. 169–184.

Brown, L.D., Zhao, W., Nelson, K.D., Hauck, M., Alsdorf, D., Ross, A., Cogan, M., Clark, M., Liu, X., Che, J., 1996. Bright spots, structure, and magmatism in southern Tibet from INDEPTH seismic reflection profiling. Science 274 (5293), 1688–1690.

Byerly, K., Brown, L., Voight, B., Miller, V., 2010. Reflection imaging of deep structure beneath Montserrat using microearthquake sources. Geophys. Res. Lett. 37 (19).

Cashman, K.V., Sparks, R.S.J., Blundy, J.D., 2017. Vertically extensive and unstable magmatic systems: a unified view of igneous processes. Science 355 (6331), eaag3055.

Cassidy, J.F., 1992. Numerical experiments in broadband receiver function analysis. Bull. Seismol. Soc. Am. 82 (3), 1453–1474.

Comeau, M.J., Unsworth, M.J., Ticona, F., Sunagua, M., 2015. Magnetotelluric images of magma distribution beneath Volcán Uturuncu, Bolivia: implications for magma dynamics. Geology 43 (3), 243–246.

Cooper, K.M., Sims, K.W., Eiler, J.M., Banerjee, N., 2016. Timescales of storage and recycling of crystal mush at Krafla Volcano, Iceland. Contrib. Mineral. Petrol. 171 (6), 54.

Darbyshire, F.A., Priestley, K.F., White, R.S., Stefánsson, R., Gudmundsson, G.B., Jakobsdóttir, S.S., 2000. Crustal structure of central and northern Iceland from analysis of teleseismic receiver functions. Geophys. J. Int. 143 (1), 163–184.

Davenport, K.K., Hole, J.A., Quiros, D.A., Brown, L.D., Chapman, M.C., Han, L., Mooney, W.D., 2015. Aftershock imaging using a dense seismometer array (AIDA) after the 2011 Mineral, Virginia, earthquake. Geol. Soc. Am. Spec. Pap. 509, SPE509–15.

de Voogd, B., Serpa, L., Brown, L., Hauser, E., Kaufman, S., Oliver, J., Troxel, B.W., Willemin, J., Wright, L.A., 1986. Death Valley bright spot: a midcrustal magma body in the southern Great Basin, California? Geology 14 (1), 64–67.

Detrick, R.S., Buhl, P., Vera, E., Mutter, J., Orcutt, J., Madsen, J., Brocher, T., 1987. Multi-channel seismic imaging of a crustal magma chamber along the East Pacific Rise. Nature 326 (6108), 35–41.

Dillon, P.B., Thomson, R.C., 1984. Offset source VSP surveys and their image reconstruction. Geophys. Prospect. 32 (5), 790–811.

Einarsson, P., 1978. S-wave shadows in the Krafla caldera in NE-Iceland, evidence for a magma chamber in the crust. Bull. Volcanol. 41 (3), 187–195.

Einarsson, P., 1991. The Krafla rifting episode 1975–1989. Náttúra Myvatns, (The Nature of Lake Myvatn), pp. 97–139.

Elders, W.A., Friþleifsson, G., Albertsson, A., 2014a. Drilling into magma and the implications of the Iceland Deep Drilling Project (IDDP) for high-temperature geothermal systems worldwide. Geothermics 49, 111–118.

Elders, W.A., Friþleifsson, G.Ó., Pálsson, B., 2014b. Iceland Deep Drilling Project: The first well, IDDP-1, drilled into magma. Geothermics 49, 1.

Friðleifsson, G.Ó., Ármannsson, H., Guðmundsson, Á., Árnason, K., Mortensen, A.K., Pálsson, B., Einarsson, G.M., 2014. Site selection for the well IDDP-1 at Krafla. Geothermics 49 (Suppl. C):9–15. https://doi.org/10.1016/j.geothermics.2013.06.001.

Greenfield, T., White, R.S., 2015. Building icelandic igneous crust by repeated melt injections. J. Geophys. Res. Solid Earth 120 (11), 7771–7788.

Hardage, B.A., 2000. In: Helbigand, K., Treitel, S. (Eds.), Vertical Seismic Profiling: Principles, Handbook of Geophysical Exploration: Seismic Exploration, 3rd ed. Elsevier Science, Oxford, U. K.

Hasegawa, A., Yamamoto, A., 1994. Deep, low-frequency microearthquakes in or around seismic low-velocity zones beneath active volcanoes in northeastern Japan. Tectonophysics 233 (3), 233–252.

IMAGE, 2016. IMAGE-D4.02 – Summary Report of WP 4.02: Active Seismic With VSP.

Inamori, T., Horiuchi, S., Hasegawa, A., 1992. Location of mid-crustal reflectors by a reflection method using aftershock waveform data in the focal area of the 1984 Western Nagano Prefecture Earthquake. J. Phys. Earth 40 (2), 379–393.

ISOR, 2014. Seismic Monitoring at Krafla: For the Period of October 2013 to October 2014, Project no: 14-0089.

Jaxybulatov, K., Shapiro, N.M., Koulakov, I., Mordret, A., Landès, M., Sens-Schönfelder, C., 2014. A large magmatic sill complex beneath the Toba caldera. Science 346 (6209): 617–619. https://doi.org/10.1126/science.1258582.

Jeddi, Z., Tryggvason, A., Gudmundsson, Ó., 2016. The Katla volcanic system imaged using local earthquakes recorded with a temporary seismic network. J. Geophys. Res. Solid Earth 121 (10), 2016JB013044. https://doi.org/10.1002/2016JB013044.

Kent, G.M., Harding, A.J., Orcutt, J.A., 1993. Distribution of magma beneath the East Pacific Rise between the Clipperton transform and the 9 17′ N deval from forward modeling of common depth point data. J. Geophys. Res. Solid Earth 98 (B8), 13945–13969.

Kent, G.M., et al., 2000. Evidence from three-dimensional seismic reflectivity images for enhanced melt supply beneath mid-ocean-ridge discontinuities. Nature 406 (6796), 614–618.

Kim, D., Brown, L.D., Árnason, K., Águstsson, K., Blanck, H., 2017. Magma reflection imaging in Krafla, Iceland, using microearthquake sources. J. Geophys. Res. Solid Earth 122, 5228–5242.

Lees, J.M., 2007. Seismic tomography of magmatic systems. J. Volcanol. Geotherm. Res. 167 (1), 37–56.

Lin, F.-C., Li, D., Clayton, R.W., Hollis, D., 2013. High-resolution 3D shallow crustal structure in Long Beach, California: application of ambient noise tomography on a dense seismic array. Geophysics 78 (4), Q45–Q56.

Makovsky, Y., Klemperer, S.L., Ratschbacher, L., Alsdorf, D., 1999. Midcrustal reflector on INDEPTH wide-angle profiles: an ophiolitic slab beneath the India-Asia suture in southern Tibet? Tectonics 18 (5):793–808. https://doi.org/10.1029/1999TC900022.

Marjanović, M., Carbotte, S.M., Carton, H., Nedimović, M.R., Mutter, J.C., Canales, J.P., 2014. A multi-sill magma plumbing system beneath the axis of the East Pacific Rise. Nat. Geosci. 7 (11), 825–829.

Matsumoto, S., Hasegawa, A., 1996. Distinct S wave reflector in the midcrust beneath Nikko-Shirane volcano in the northeastern Japan arc. J. Geophys. Res. Solid Earth 101 (B2), 3067–3083.

Mortensen, A.K., Grönvold, K., Gu, K., Gu, K.A., Steingrímsson, B., Egilson, T., 2010. Quenched silicic glass from well K-39 in Krafla, North-Eastern Iceland. Proceedings World Geothermal Congress, Bali, Indonesia.

Murase, T., Mcbirney, A.R., 1973. Properties of some common igneous rocks and their melts at high temperatures. Geol. Soc. Am. Bull. 84 (11), 3563–3592.

Quiros, D., Brown, L.D., Cabolova, A., Chen, C., Davenport, K., Hole, J., ... Mooney, W., 2015. Reflection imaging using earthquake sources: a novel application of reverse vertical seismic profiling (RVSP). SEG Technical Program Expanded Abstracts 2015. Society of Exploration Geophysicists, pp. 5565–5569.

Quiros, D.A., Brown, L.D., Davenport, K.K., Hole, J.A., Cabolova, A., Chen, C., ... Mooney, W.D., 2017. Reflection imaging with earthquake sources and dense arrays. J. Geophys. Res. Solid Earth 122 (4), 2016JB013677. https://doi.org/10.1002/2016JB013677.

Sanford, A.R., Long, L.T., 1965. Microearthquake crustal reflections, Socorro, New Mexico. Bull. Seismol. Soc. Am. 55 (3), 579–586.

Sanford, A.R., Alptekin, Ö., Toppozada, T.R., 1973. Use of reflection phases on microearthquake seismograms to map an unusual discontinuity beneath the Rio Grande rift. Bull. Seismol. Soc. Am. 63 (6–1), 2021–2034.

Sheetz, K.E., Schlue, J.W., 1992. Inferences for the Socorro magma body from teleseismic receiver functions. Geophys. Res. Lett. 19 (18), 1867–1870.

Sheriff, R.E., 1975. Factors affecting seismic amplitudes. Geophys. Prospect. 23 (1), 125–138.

Sveinbjornsdottir, A.E., Coleman, M.L., Yardley, B.W.D., 1986. Origin and history of hydrothermal fluids of the Reykjanes and Krafla geothermal fields, Iceland. Contrib. Mineral. Petrol. 94 (1), 99–109.
Tarasewicz, J., White, R.S., Woods, A.W., Brandsdóttir, B., Gudmundsson, M.T., 2012. Magma mobilization by downward-propagating decompression of the Eyjafjallajökull volcanic plumbing system. Geophys. Res. Lett. 39, 19.
Tromp, J., Komattisch, D., Liu, Q., 2008. Spectral-element and adjoint methods in seismology. Commun. Comput. Phys. 3 (1), 1–32.
Unsworth, M.J., Jones, A.G., Wei, W., Marquis, G., Gokarn, S.G., Spratt, J.E., others, …., 2005. Crustal rheology of the Himalaya and Southern Tibet inferred from magnetotelluric data. Nature 438 (7064), 78–81.
Walton, G.G., 1972. Three-dimensional seismic method. Geophysics 37 (3), 417–430.
Wei, W., Unsworth, M., Jones, A., Booker, J., Tan, H., Nelson, D., Chen, L., Li, S., Solon, K., Bedrosian, P., Jin, S., Deng, M., Ledo, J., Kay, D., Roberts, B., 2001. Detection of widespread fluids in the Tibetan crust by magnetotelluric studies. Science 292 (5517), 716–719.
Wilson, D., Aster, R., West, M., Ni, J., et al., 2005. Lithospheric structure of the Rio Grande rift. Nature 433 (7028), 851.
Yilmaz, Ö., 2001. Seismic Data Analysis. Society of Exploration Geophysicists.
Zandt, G., Leidig, M., Chmielowski, J., Baumont, D., Yuan, X., 2003. Seismic detection and characterization of the Altiplano-Puna magma body, central Andes. Pure Appl. Geophys. 160 (3–4), 789–807.